optimally doped case (solid line). It is interesting to note that the peak in the underdoped case is slightly reduced in height reflecting a reduction in T_c. It is also shifted to lower energies. Some experiments[19] indicate a reduction in gap value with underdoping in YBCO while many experiments show an important increase in Bi2212 (ref. 18). Even if the gap is assumed to stay the same at 27 meV, the spin-polarized neutron-resonant frequency is known to decrease with doping[20]. Accounting for this gives almost exactly the downward shift observed in our experimental data of Fig. 2b.

Recent inelastic neutron scattering data in Bi2212 (ref. 21) show a resonance peak at 43 meV in the superconducting state and establish a similarity with the earlier results in YBCO. We have inverted the optical data of Puchkov *et al.*[4] in this case and find that coupling at low temperatures to the observed superconducting-state spin-resonance peak is a general phenomenon in both YBCO and Bi2212.

Spin excitations are thus seen in an appropriately chosen second derivative of the superconducting state optical conductivity, and hence the strength of their coupling to the charge carriers is determined. The coupling to the excitations including the 41 meV resonance is large enough in YBCO to account for superconductivity at that temperature. At T_c the spectrum obtained from experiment[4] gives a value of the mass enhancement parameter λ which is close to the value used in our model calculations to obtain a critical temperature of 100 K.

Note added in proof: While this paper was in press, we became aware of a related theoretical study by Munzar, D. *et al.*, *Physica C* **312,** 121–135 (1999). □

Received 3 June; accepted 27 July 1999.

1. McMillan, W. L. & Rowell, J. M. Lead phonon spectrum calculated from superconducting density of states. *Phys. Rev. Lett.* **14,** 108–112 (1965).
2. Carbotte, J. P. Properties of boson exchange superconductors. *Rev. Mod. Phys.* **62,** 1027–1157 (1990).
3. Marsiglio, F. *et al.* Inversion of K_3C_{60} reflectance data. *Phys. Lett. A* **245,** 172–176 (1998).
4. Puchkov, A. V. *et al.* High T_c superconductors: an infrared study. *J. Phys.* **8,** 10049–10082 (1996).
5. Bourges, P. in *The Gap Symmetry and Fluctuations in High Temperature Superconductors* (ed. Bok. J. *et al.*) 349–374 (Plenum, 1998).
6. Scalapino, D. J. *et al.* *d*-Wave pairing near a spin-density-wave instability. *Phys. Rev. B* **34,** 8190–8192 (1986).
7. Monthoux, P. & Pines, D. YBCO: a nearly antiferromagnetic Fermi liquid. *Phys. Rev. B* **47,** 6069–6081 (1993).
8. Wollman, D. A. *et al.* Experimental determination of the superconducting pairing state in YBCO from the phase coherence of YBCO–Pb dc SQUIDs. *Phys. Rev. Lett.* **71,** 2134–2137 (1993).
9. Tsuei, C. C. *et al.* Pairing symmetry and flux quantization in a tricrystal superconducting ring of YBCO. *Phys. Rev. Lett.* **73,** 593–596 (1994).
10. Bourges, P. *et al.* Spin dynamics in high-T_c superconductors. (Preprint cond-mat/9902067).
11. Bulut, N. & Scalapino, D. J. Neutron scattering from a collective spin fluctuation mode in a CuO_2 bilayer. *Phys. Rev. B* **53,** 5149–5152 (1996).
12. Demler, E. & Zhang, S. C. Theory of the resonant neutron scattering of high-T_c superconductors. *Phys. Rev. Lett.* **75,** 4126–4129 (1995).
13. Nuss, M. C. *et al.* Dynamic conductivity and 'coherence peak' in $YBa_2Cu_3O_7$ superconductors. *Phys. Rev. Lett.* **66,** 3305–3308 (1991).
14. Varma, C. M. *et al.* Phenomenology of the normal state of Cu–O high temperature superconductors. *Phys. Rev. Lett.* **63,** 1996–1999 (1989).
15. Schachinger, E. *et al.* Suppression of inelastic scattering on penetration depth and conductivity in $d_{x^2-y^2}$ superconductors. *Phys. Rev. B* **56,** 2738–2750 (1997).
16. Basov, D. N. *et al.* Pseudogap and charge dynamics in CuO_2 planes in YBCO. *Phys. Rev. Lett.* **77,** 4090–4093 (1996).
17. Collins, R. T. *et al.* Reflectivity and conductivity of $YBa_2Cu_3O_7$. *Phys. Rev. B* **39,** 6571–6574 (1989).
18. DeWilde, Y. *et al.* Unusual strong coupling effects in the tunneling spectroscopy of optimally doped and overdoped $Bi_2Sn_2CaCu_2O_{8+\delta}$. *Phys. Rev. Lett.* **80,** 153–156 (1998).
19. Ponomarev, Yo. G. *et al.* Josephson effect and single particle tunneling in YBCO and YBCO single crystal break junctions. *Physica C* **243,** 167–176 (1995).
20. Fong, H. F. *et al.* Superconducting-induced anomalies in the spin excitation spectra of underdoped YBCO. *Phys. Rev. Lett.* **78,** 713–716 (1997).
21. Fong, H. F. *et al.* Neutron scattering from magnetic excitations in $Bi_2Sr_2CaCu_2O_{8+\delta}$. *Nature* **398,** 588–591 (1999).

Acknowledgements

This work was supported in part by the Natural Sciences and Engineering Research Council of Canada (NSERC) and the Canadian Institute for Advanced Research (CIAR). Work at University of California at San Diego (UCSD) is supported by the NFS 'Early Career Development' programme. DNB is a Cottrel Scholar of the Research Corporation. We thank J. E. Hirsch, P. B. Hirschfeld, P. B. Littlewood, F. Marsiglio, E. J. Nicol, D. Scalapino, T. Timusk, and I. Vekhter for interest.

Correspondence and requests for materials should be addressed to E.S. (e-mail: Schachinger@itp.tu-graz.ac.at).

Coupled ocean–atmosphere dynamics in the Indian Ocean during 1997–98

Peter J. Webster*, Andrew M. Moore*, Johannes P. Loschnigg* & Robert R. Leben†

** Program in Atmospheric and Oceanic Sciences, Campus Box 311, University of Colorado, Boulder, Colorado 80309-311, USA*
† Colorado Center for Astrodynamics Research, Department of Aerospace Engineering Sciences, University of Colorado, Boulder, Colorado 80309-311, USA

Climate variability in the Indian Ocean region seems to be, in some aspects, independent of forcing by external phenomena such as the El Niño/Southern Oscillation[1–4]. But the extent to which, and how, internal coupled ocean–atmosphere dynamics determine the state of the Indian Ocean system have not been resolved. Here we present a detailed analysis of the strong seasonal anomalies in sea surface temperatures, sea surface heights, precipitation and winds that occurred in the Indian Ocean region in 1997–98, and compare the results with the record of Indian Ocean climate variability over the past 40 years. We conclude that the 1997–98 anomalies—in spite of the coincidence with the strong El Niño/Southern Oscillation event—may primarily be an expression of internal dynamics, rather than a direct response to external influences. We propose a mechanism of ocean–atmosphere interaction governing the 1997–98 event that may represent a characteristic internal mode of the Indian Ocean climate system. In the Pacific Ocean, the identification of such a mode has led to successful predictions of El Niño[5]; if the proposed Indian Ocean internal mode proves to be robust, there may be a similar potential for predictability of climate in the Indian Ocean region.

A strong, cool sea surface temperature (SST) anomaly (with respect to the 1950–97 mean as calculated from ref. 6) developed in the eastern Indian Ocean in July 1997 and reached a maximum (>−2 °C) in November 1997 (Fig. 1a). At about the same time, starting in June 1997, a warm SST anomaly developed in the western Indian Ocean, with a maximum of >+2 °C in February 1998. Together, these heating and cooling anomalies produced a reversed SST gradient (SST increasing east to west) between November 1997 and June 1998 relative to the climatological temperature gradient (SST increasing west to east). Following the appearance of warm SST anomalies off the east African coast in June 1997, the usually weak climatological equatorial westerly winds (calculated from the NCEP/NCAR near-surface zonal wind component[7]) were replaced by surface easterly winds. The wind anomalies exceeded $-5\ m\ s^{-1}$ over the central equatorial Indian Ocean in December 1997 (Fig. 1b). Between July 1997 and May 1998, the sea surface height (SSH) was depressed substantially in the eastern basin, compared to the mean value as described in ref. 8, and generally higher in the west. Maximum height differences along the equator exceeded 30 cm between November 1997 and May 1998 (Fig. 1c). These variations in the climate of the Indian Ocean sector have been noted elsewhere[9]. Usually, Indian Ocean SST variations associated with El Niño are ~0.5 °C, but exhibit very different patterns to that noted in Fig. 1a (ref. 10).

The spatial distribution of deviations from the long-term mean SST, the outgoing longwave radiation (OLR, as a proxy for rainfall), the surface zonal wind velocity for November 1997, and the SSH field for the period November 20–30 1997, are shown in Fig. 2a–d (the long-term mean fields of SST, OLR and near-surface wind, see Figs 1–3 in Supplementary Information). There is a clear spatial structure in the anomalous SST fields, with extreme values in the

eastern and western regions of the basin. Compared to the long-term average, the near-surface anomalous zonal wind fields point strongly to the east (>−6 m s^{-1}) with the core located just south of the Equator between 60° E and 100° E (Fig. 2c). Usually the zonal winds in autumn (September–November) are weak westerlies (see Fig. 3 in Supplementary Information). Fields of OLR measured by satellites provide the black-body radiating temperature of the atmosphere. Low OLR values indicate emissions from the upper troposphere and, thus, from deep convective clouds which are mainly responsible for rain in the tropics. High values of OLR, on the other hand, signal emission from the low troposphere and indicate an absence of deep convective clouds[11]. Thus, the OLR distribution in Fig. 2b depicts greater than average rainfall in the western and northwestern Indian Ocean and diminished rainfall in the east. Along the Equator there is an OLR gradient of ~70 W m^{-2}—roughly the same magnitude as between the western and eastern Pacific Ocean, but over half the horizontal distance. The OLR gradient is consistent with an atmospheric circulation having strong rising motion above the western Indian Ocean, strong surface flow to the west and subsidence in the east[12,13]. Analyses of the NCEP/NCAR data substantiates the existence of the strong longitudinal cell[14]. The SSH field (Fig. 2d) shows lower values in the east, especially near Sumatra, and higher values in the west. To the south of the Equator and in the central and western Indian Ocean there is an elongated 'ridge' some 30 cm above adjacent ocean regions. The location and magnitude of the ridge is consistent

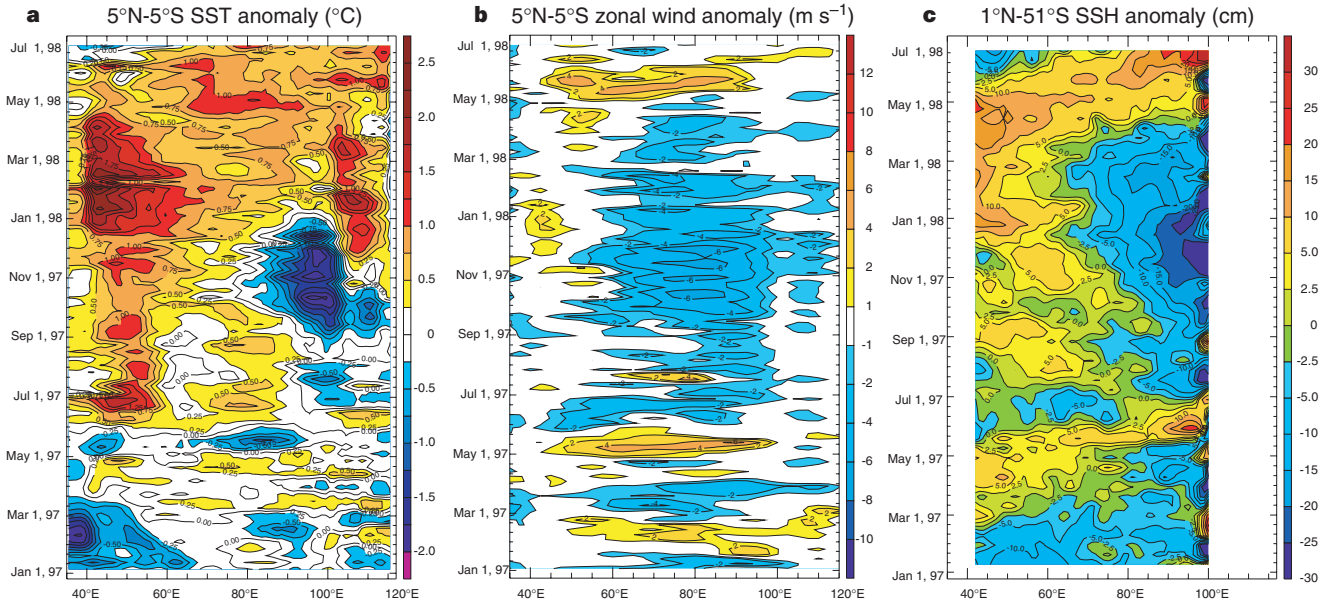

Figure 1 Evolution of the state of the Indian Ocean, 1997–98. Panels **a** and **b** show the anomalous SST and the zonal wind anomaly at the surface, respectively, averaged between 5° N and 5° S. The average annual cycle has been removed. Panel **c** shows the SSH field obtained from TOPEX/POSEIDON averaged between 1° N and 1° S. The ordinate month marker denotes the beginning of the month.

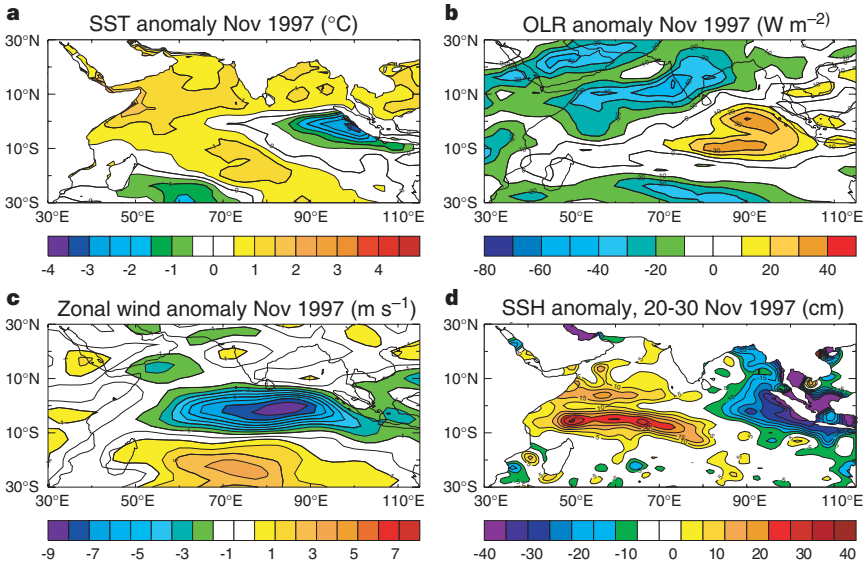

Figure 2 State of the Indian Ocean in November 1997. Panels show the latitude–longitude sections of anomalous (long-term monthly average removed) SST (**a**), outgoing longwave radiation (OLR) as determined from a satellite, which is a surrogate for precipitation (**b**), the zonal component of the surface wind field (**c**), and the surface height determined from TOPEX/POSEIDON for 20–30 November 1997 (**d**).

with Southern Hemisphere Ekman mass transports to the left of the surface equatorial easterlies and westerlies near 10° S.

The time evolution of this ridge of elevated sea level south of the Equator is shown in Fig. 3. Longitude-time sections of SSH anomalies averaged between 4° and 6° S (Fig. 3a) and between 11° and 13° S (Fig. 3b) are shown for the period 1 January 1997 to 30 June 1998. Westward propagation of the ridge is evident at both latitudes, with lower westward phase speeds at higher latitudes. The westward phase speed and its decrease with increasing latitude suggests that ocean Rossby waves are important in the development and propagation of the ridge. Figure 3b also shows the emergence of Rossby waves from the eastern boundary around the time that winds are observed to increase along the coast of Sumatra, as discussed below. The timing, formation and the propagation of dynamical features of the Ekman ridge have been simulated with some accuracy by a simple one-and-a-half layer Gill-type model[15] driven by observed surface wind fields. Analysis of the model results shows that the westward propagating modes are ocean downwelling Rossby waves.

Many of the changes observed in the SST and SSH fields can be explained by changes in the surface winds. Beginning in the late summer of 1997, the alongshore component of the surface winds off Sumatra were 2–3 m s^{-1} stronger than normal to the northwest and were conducive to increased coastal upwelling, illustrated schematically in Fig. 4a. Starting in late summer, the alongshore winds off the African coast were weaker to the southwest by 2 m s^{-1}, which resulted in a reduction in upwelling south of the Equator. Initially, the warmer SSTs in the western Indian Ocean starting in June 1997 produced easterly wind anomalies over the central Indian Ocean that would later be enhanced by the cooler temperatures in the eastern basin. The accelerating equatorial easterlies would promote a large-scale dynamic adjustment of the SSH along the Equator, leading to a shallower eastern thermocline and a deeper western thermocline.

We suggest that the anomalous state in the Indian Ocean that we describe above may not have been an exaggerated response to the strong 1997–98 El Niño. There are a number of reasons for this suggestion. First, the climate pattern around the Indian Ocean rim was very different during 1997–98 from that usually associated with a Pacific warm event. The drought in Indonesia was more intense than anticipated, the rainfall in the 1997 Indian summer monsoon and over Australia was near normal (although drought is usually expected in both regions), and the east African rainfall, usually only slightly higher during an El Niño, was the largest this century. Second, the typical El Niño/Southern Oscillation (ENSO) cycle appears more associated with a general warming of the equatorial Indian Ocean than a change in the longitudinal SST gradient, probably due to the lighter than average winds that occur over the Indian Ocean during an El Niño[10,16]. The correlations, *R*, between the mean equatorial SST in the Indian Ocean and ENSO is +0.52, but falls to non-significant values of +0.19 between ENSO and the equatorial SST gradient. The correlation between October–November east African rainfall and the along-Equator Indian Ocean SST gradient is +0.62, indicating a relatively strong relationship between these two time series from within the Indian Ocean basin. Circulation and SST patterns in 1997–98 were similar to previous extremes in the east African rainfall (see Fig. 4a in Supplementary Information). The correlation between east African rainfall and the central Pacific SST anomalies, however, is only 0.24, indicating a rather weak relationship between east African rainfall and ENSO. In support of our findings, previous studies of African rainfall[17,18] have suggested that other factors besides ENSO are responsible for east African rainfall variability. Third, similar excursions from normal have occurred in the Indian Ocean in the absence of ENSO extrema. During 1961–62, the SST gradient across the Indian Ocean reversed, with substantial warming in the western basin[19,20]. In all, between 1950 and 1998 there were 16 years in which the equatorial SST gradient reversed for at least a month. Of these years, only three were El Niño years. None coincided with a La Niña. Spectral analysis of the time series of the along-Equator SST gradient (see Fig. 5 in Supplementary Information) shows peaks in a broad band around 2 years (exceeding 87% confidence limits) and 5 years (exceeding

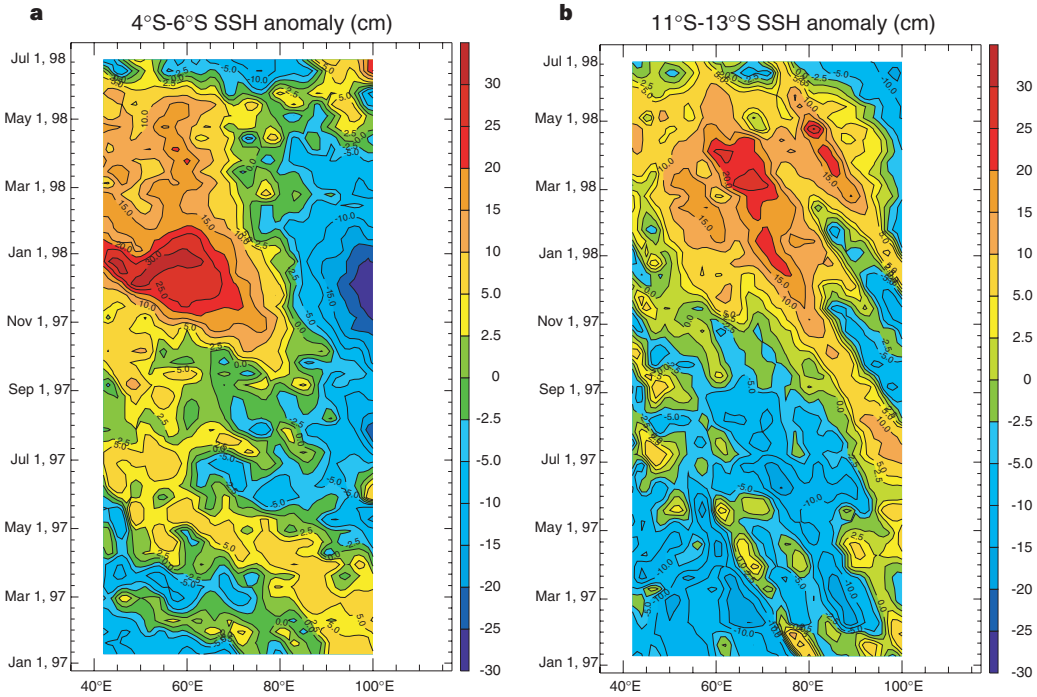

Figure 3 The evolving sea surface height (SSH) field. Panels show time–longitude sections of anomalous SSH obtained from TOPEX/POSEIDON averaged between 4° S and 6° S (**a**), and between 11° S and 13° S (**b**). Note the differential westward propagation as a function of latitude. As latitude increases the phase speed decreases, consistent with the propagation characteristics of an ocean Rossby wave.

97%), indicating long-period oscillations in the gradient between two anomalous states: warm in the west and cool in the east, and cool in the west and warm in the east.

The possible sequence of events in the Indian Ocean occurring once the east–west equatorial SST gradient was established is shown in Fig. 4b–d. With a source of moist air from the Indian Ocean, strong convection develops over the heated land mass of east Africa during autumn of 1997, enhancing the equatorial easterly flow (Fig. 4b). Ekman transports, driven by the easterly anomalies, produce the Ekman ridge just south of the Equator. In seeking equilibrium, ocean Rossby wave dynamics cause the ridge to propagate westward which, in turn, deepens the thermocline to the west of the source of the Ekman convergence (Fig. 4c). With a deeper thermocline and reduced upwelling, the western Indian Ocean continued to warm, thus maintaining the driving force of the anomalous easterly surface winds. In this manner, the Ekman ridge is sustained, allowing for a continual eastward propagation of the equatorial ocean Rossby waves. We propose that this self-sustaining system prolonged the warming in the western basin by a number of months.

A warming period may end, or diminish, in a number of ways. For example, a warm west Indian Ocean is often associated with a strong monsoon[21,22]. This means that the summer monsoon following the Indian Ocean warming should have stronger winds in the western basin, which would induce greater mixing, greater Ekman transports forcing coastal upwelling, and greater evaporation, all of which would contribute to rapid cooling. Also, as the El Niño weakens (as it did during the spring of 1998), and the locus of convection moves back towards Indonesia, the equatorial wind patterns in the Indian Ocean revert to westerlies (Fig. 4d). The

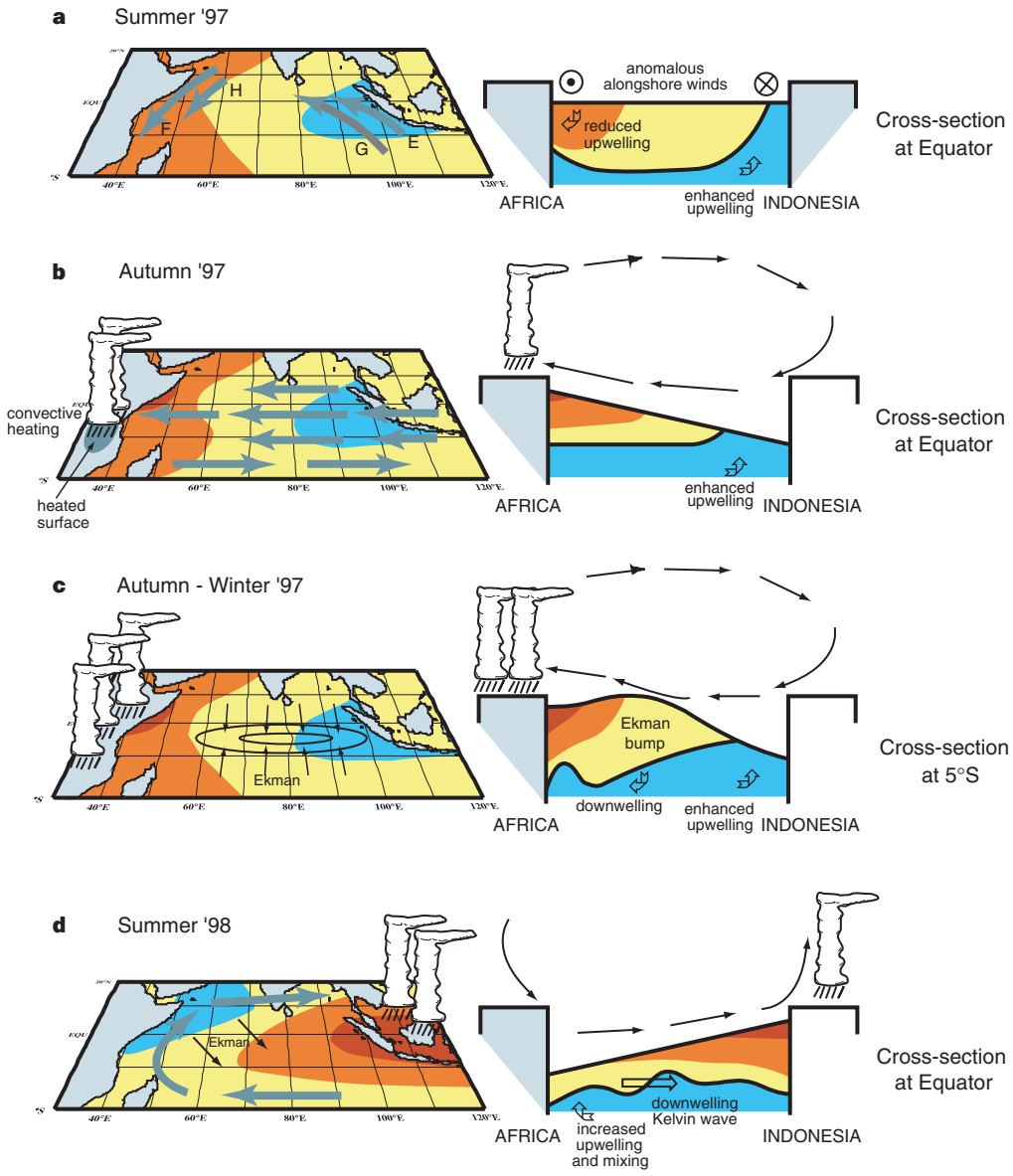

Figure 4 Diagram of the sequence of events in 1997–98. **a**, The climatological alongshore winds off Sumatra (E) and the east African coast (F). The winds observed in the late summer and early autumn are denoted by G and H, respectively. The right-hand panel shows the effect at the Equator on the upper ocean induced by increased upwelling in the east and decreased upwelling in the west. Wind into and out of the plane of the paper are denoted by the bull's eye and cross-hair symbols, respectively. **b**, Distribution of the winds resulting from the anomalous SST gradient along the Equator and the changes in the SSH distribution. **c**, Formation of the Ekman ridge in the central Indian Ocean and the forcing of westward-propagating downwelling equatorial Rossby waves to the west. The right-hand panel shows the effect on the upper ocean near 5° S. **d**, Subsequent cooling of the western Indian Ocean through enhanced mixing and coastal Ekman transports from stronger than average monsoon winds and through circulation changes associated with the weakening of the 1997–98 El Niño.

resulting relaxation of the SSH fields would force eastward-propagating and downwelling Kelvin waves which would deepen the eastern mixed layer and return the system to a normal configuration. These changes may be seen in the spring and early summer of 1998 in Fig. 1.

The results presented above suggest that the Indian Ocean exhibits strong coupled ocean–atmosphere–land interactions that are self-maintaining, and are capable of producing significant perturbations to the annual cycle, at least during the 1997–1998 period. Arguably, the evolution of the perturbation is independent of ENSO. We note that other hypotheses[3,4] have been suggested for observed interannual variability in the Indian Ocean. These theories rely on the Indian Ocean responding locally to either weaker or stronger monsoon winds which, through changes in upwelling and mixing, introduce a biennial component to the system. But the weakness of these theories is the maintenance of the upper-ocean anomalies from year to year. Our hypothesis adds a coupled dynamical component that has a longer timescale than the thermodynamics of the mixed layer, and which may form a link from one monsoon season to the next. Thus we suggest that the Indian Ocean may not be a passive player in climate variability on seasonal to interannual timescales, but may enact a very active and independent role. □

Received 6 July 1998; accepted 9 July 1999.

1. Nicholls, N. Air-sea interaction and the quasi-biennial oscillation. *Mon. Weath. Rev.* **106,** 1505–1508 (1983).
2. Nicholls, N. All-India summer monsoon rainfall and sea surface temperature around northern Australia and Indonesia. *J. Clim.* **8,** 1463–1467 (1995).
3. Meehl, G. A. Coupled ocean-atmosphere-land processes and south Asian monsoon variability. *Science* **265,** 263–267 (1994).
4. Meehl, G. A. The south Asian monsoon and the tropospheric biennial oscillation. *J. Clim.* **10,** 1921–1943 (1997).
5. Webster, P. J. & Palmer, T. N. The past and future of El Niño. *Nature* **390,** 562–564 (1997).
6. Reynolds, R. & Marisco, D. An improved real-time global sea surface temperature analysis. *J. Clim.* **6,** 114–119 (1993).
7. Kalnay, E. *et al.* The NCEP/NCAR 40-year reanalysis project. *Bull. Am. Meteorol. Soc.* **77,** 437–471 (1996).
8. Hendricks, J. R., Leben, R. R., Born, G. H. & Koblinsky, C. J. Empirical orthogonal function analysis of global TOPEX/POSEIDON altimeter data and implications for detection of global sea level rise. *J. Geophys. Res.* **101,** 14131–14145 (1996).
9. Yu, L. & Rienecker, M. M. Mechanisms for the Indian Ocean warming during the 1997–1998 El Niño. *Geophys. Res. Lett.* **26,** 735–738 (1999).
10. Barnett, T. P. Interaction of the monsoon and Pacific Ocean trade wind systems at interannual time scales. Part I: the equatorial zone. *Mon. Weath. Rev.* **111,** 756–773 (1983).
11. Arkin, P. & Meisner, B. The relationship between large-scale convective rainfall and cloud cover over the western hemisphere during 1982–1984. *Mon. Weath. Rev.* **115,** 51–74 (1987).
12. Webster, P. J. Response of the tropical atmosphere to local steady forcing. *Mon. Weath. Rev.* **100,** 518–541 (1972).
13. Gill, A. E. Some simple solutions for heat-induced tropical circulation. *Q. J. R. Meteorol. Soc.* **106,** 447–462 (1981).
14. *Near Real-Time Analysis of the Ocean and Atmosphere* Fig T 29, p. 36 (Climate Diagnostics Bull. NO. 97/11, Climate Diagnostics Center, National Center of Environmental Prediction, NOAA, Washington DC, 1997).
15. Gill, A. *Atmosphere-Ocean Dynamics* (Academic, London, 1982).
16. Webster, P. J. *et al.* Monsoons: processes, predictability and the prospects for prediction. *J. Geophys. Res.* **103,** 14451–14510 (1998).
17. Nicholson, S. E. & Kim, J. The relationship of the El-Niño Southern Oscillation to African rainfall. *Int. J. Climatol.* **17,** 117–135 (1997).
18. Nicholson, S. E. An analysis of the ENSO signal in the tropical Atlantic and western Indian Oceans. *Int. J. Climatol.* **17,** 345–375 (1997).
19. Reverdin, G., Cadet, D. & Gutzler, D. Interannual displacements of convection and surface circulation over the equatorial Indian Ocean. *Q. J. R. Meteorol. Soc.* **122,** 43–67 (1986).
20. Kapala, A., Born, K. & Flohn, H. in *Proc. Int. Conf. on Monsoon Variability and Prediction* (ed. Newson, R.) 119–126 (Tech. Doc. 619, World Meteorological Organization, Geneva, Switzerland, 1994).
21. Rao, K. G. & Goswami, B. N. Interannual variations of the sea-surface temperature over the Arabian Sea and the Indian Monsoon: A new perspective. *Mon. Weath. Rev.* **116,** 558–568 (1988).
22. Shukla, J. & Mooley, D. A. Empirical prediction of the summer monsoon over India. *Mon. Weath. Rev.* **115,** 695–703 (1987).

Supplementary information is available on *Nature*'s World-Wide Web site (http://www.nature.com) or as hard copy from the London editorial office of *Nature*.

Acknowledgements

This work was supported by the Office of Global Programs, NOAA, and the NSF (P.J.W., A.M.M., J.P.L.), and by NASA (R.R.L.).

Correspondence and requests for materials should be addressed to P.J.W. (e-mail: pjw@oz.colorado.edu).

A dipole mode in the tropical Indian Ocean

N. H. Saji*, B. N. Goswami†, P. N. Vinayachandran* & T. Yamagata*‡

** Institute for Global Change Research, SEAVANS N 7F, 1-2-1 Shibaura, Minato-ku, Tokyo 105 6791, Japan*
† Center for Atmospheric and Oceanic Sciences, Indian Institute of Science, Bangalore 560 012, India
‡ Department of Earth and Planetary Physics, Graduate School of Science, The University of Tokyo, Tokyo 113 0033, Japan

For the tropical Pacific and Atlantic oceans, internal modes of variability that lead to climatic oscillations have been recognized[1,2], but in the Indian Ocean region a similar ocean–atmosphere interaction causing interannual climate variability has not yet been found[3]. Here we report an analysis of observational data over the past 40 years, showing a dipole mode in the Indian Ocean: a pattern of internal variability with anomalously low sea surface temperatures off Sumatra and high sea surface temperatures in the western Indian Ocean, with accompanying wind and precipitation anomalies. The spatio-temporal links between sea surface temperatures and winds reveal a strong coupling through the precipitation field and ocean dynamics. This air–sea interaction process is unique and inherent in the Indian Ocean, and is shown to be independent of the El Niño/Southern Oscillation. The discovery of this dipole mode that accounts for about 12% of the sea surface temperature variability in the Indian Ocean—and, in its active years, also causes severe rainfall in eastern Africa and droughts in Indonesia—brightens the prospects for a long-term forecast of rainfall anomalies in the affected countries.

The catastrophic rains of 1961 in tropical eastern Africa and subsequent abrupt discharge of the White Nile are now known[4–6] to be part of an anomalous climate state over the tropical Indian Ocean. A dipole structure characterized the sea surface temperature (SST) anomaly during this event: warmer than usual SSTs occurred over large parts of the western basin, while SSTs off Sumatra were cooler than usual. Rainfall increased over tropical eastern Africa and the western Indian Ocean, while over the Indonesian archipelago it decreased, resulting in severe drought. Equatorial surface winds, which in a normal summer season blow towards the east, weakened and reversed direction. There was no El Niño in the Pacific, while India experienced the highest summer monsoon rainfall in the past 150 years (ref. 5). By examining long-term data sets of SST

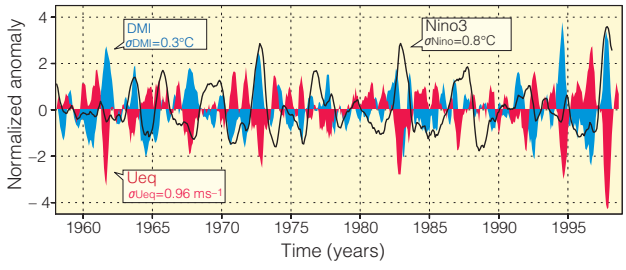

Figure 1 Dipole mode and El Niño events since 1958. Plotted in blue, the dipole mode index (DMI) exhibits a pattern of evolution distinctly different from that of the El Niño, which is represented by the Nino3 sea surface temperature (SST) anomalies (black line). On the other hand, equatorial zonal wind anomalies U_{eq} (plotted in red) coevolves with the DMI. All the three time series have been normalized by their respective standard deviations. We have removed variability with periods of 7 years or longer, based on harmonic analysis, from all the data sets used in this analysis. In addition, we have smoothed the time series using a 5-month running mean.